Design and Optimization of a Tri-Band Rectenna for 3G, 4G and 5G RF Energy Harvesting Using Characteristic Mode Analysis

Vijay S[1*], Ashok Bakkiyaraj R[2], Mohamed Ismail M[3]

[1] Research Scholar, Dept. Electrical Engineering, Annamalai University, Chidambaram, Tamil Nadu, India, s.vijayeee@gmail.com
[2] Associate Professor, Dept. Electrical Engineering, Annamalai University, Chidambaram, Tamil Nadu, India, auashok@gmail.com
[3] Professor, Dept. Electronics and Communication Engineering, Crescent Institute of Science & Technology, Chennai, Tamil Nadu, India, mmismail@crescent.education

KEYWORDS
3G, 4G, 5G
Sub-6,
Tri-Band Antenna,
Rectenna,
Characteristic Mode Analysis,
RF Energy Harvesting

Abstract. This research paper focuses on designing and analysing a tri-band antenna for RF energy harvesting within the sub-6 GHz spectrum, specifically targeting 2.1 GHz (3G), 2.3 GHz (4G), and 3.5 GHz (5G). The antenna structure incorporates three dipole elements that resonate at distinct frequencies while maintaining a compact footprint. Characteristic Mode Analysis (CMA) is applied to refine the antenna design, improving its radiation efficiency and ensuring enhanced broadside performance. The antenna's performance is evaluated through simulated and measured S_{11} parameters and radiation patterns. A tri-band bandpass filter is integrated into the system to enhance impedance matching across the 2.1 GHz, 2.3 GHz, and 3.5 GHz bands, ensuring efficient signal transfer at each operational frequency. Additionally, an RF-to-DC rectification circuit is designed using a Schottky diode alongside a low-pass filter and load resistor, enabling effective conversion of ambient RF signals into usable DC power for energy harvesting applications. The results obtained from this study validate the tri-band antenna's capability to efficiently harvest RF energy within the 3G, 4G, and 5G frequency ranges. By leveraging Characteristic Mode Analysis (CMA), the proposed design optimizes radiation efficiency, while the rectifier circuit exhibits stable RF-to-DC conversion across different power levels.

1. Introduction

The rapid expansion of wireless communication networks has led to the continuous emission of electromagnetic (EM) waves from sources such as cellular base stations, Wi-Fi routers, satellite links, and Internet of Things (IoT) devices. While these signals are typically regarded as lost energy, they can instead be harnessed and converted into electrical power, providing an alternative and sustainable energy source for low-power electronic devices [1-5]. This study aims to optimize RF energy harvesting by improving antenna design, ensuring better efficiency and adaptability for real-world applications. Free electromagnetic energy harvesting (EMEH) has gained significant attention as an alternative energy solution for powering battery-less wireless sensors, wearable electronics, and remote monitoring devices. By utilizing ambient RF signals, this technology reduces reliance on conventional batteries, minimizing maintenance efforts and enhancing system longevity [6-8].

The applications of electromagnetic energy harvesting extend across various sectors. In wireless sensor networks (WSNs), it facilitates autonomous sensor nodes, reducing dependence on regular battery replacements [9]. For IoT-based smart cities, RF energy harvesting provides power for smart meters, environmental sensors, and industrial automation systems. Additionally, in healthcare, wearable monitoring devices and biomedical sensors benefit from a continuous and sustainable power supply. Moreover, autonomous systems such as UAVs, satellites, and remote communication stations can leverage harvested RF energy to extend operational capabilities without frequent human intervention [10-14].

There are different methods of RF energy harvesting, primarily categorized into passive, active, and hybrid techniques. Passive RF energy harvesting relies on ambient electromagnetic waves from existing communication infrastructure, where an antenna captures these signals, which are then converted into DC power using a rectifier circuit. Active RF energy harvesting involves dedicated RF power transmission from a source to a receiving antenna, ensuring optimized energy transfer. Hybrid energy harvesting combines RF with other energy sources, such as solar or thermoelectric generation, enhancing the total energy output and making the system more reliable. A typical RF energy harvesting system consists of an antenna to capture RF signals, a matching network to optimize impedance, a rectifier circuit to convert RF signals into DC power, and an energy storage unit like a supercapacitor or battery for long-term use [14-18].

Several studies have explored different aspects of RF energy harvesting, focusing on improving efficiency, bandwidth, and miniaturization. Various antenna configurations, such as dipole, patch, and fractal antennas, have been investigated to enhance RF energy capture across multiple frequency bands. Multi-band and broadband antennas have been proposed to maximize energy harvesting from different sources simultaneously. Additionally, significant research has been conducted on rectifier circuit optimization, where Schottky diodes, CMOS rectifiers, and impedance-matching techniques have been employed to improve RF-to-DC conversion efficiency. Advanced rectification techniques, such as voltage multiplication and differential rectification, have further enhanced power conversion. Moreover, hybrid energy harvesting systems combining RF with solar or vibrational energy sources have been explored to improve overall energy output for IoT and remote sensing applications. Despite these advancements, challenges such as impedance mismatch, low conversion efficiency, and limited power output remain key areas of research [18-19].

Beyond stationary sensor nodes, sustainable RF energy harvesting for wearables and biomedical electronics is rapidly advancing. The integration of innovative materials and flexible architectures, as highlighted by Patel et al. (2025), enables self-powered devices with improved adaptability, reliability, and long-term energy autonomy for next-generation medical and environmental monitoring networks. This opens the door for new classes of ultra-low-power, portable electronics, directly addressing practical deployment scenarios in health and smart environments.[20]

Recent advances in microstrip antenna technology for IoT and 5G applications have demonstrated the potential of innovative fabrication methods and design approaches to enhance antenna performance and versatility. For example, 3D-printed microstrip antennas enable symbiotic communication through WiFi backscatter and exhibit flexible bit rate evaluation tailored for IoT environments [21]. Compact dual-band antennas with metamaterial integration further show promise for next-generation IoT applications by utilizing advanced wireless communication techniques [22]. Additionally, novel machine learning-driven approaches are emerging, allowing for rapid optimization and design of multi-band patch antennas customized for 5G/6G IoT scenarios [23]. Compact inset-feed microstrip antennas for 5G and smart city IoT infrastructure exemplify the practical relevance of integrating such designs in future wireless systems [24]. In addition to traditional sub-6 GHz solutions, slotted patch antennas explicitly designed for the Wi-Fi 6E extended frequency band now offer substantial improvements. A recent work of Alam et al. (2025) demonstrated an antenna with exceptional impedance matching, wide operational bandwidth, and over 53% energy harvesting efficiency. Such designs prove highly suitable for environments with dynamic RF spectra, enhancing the feasibility of autonomous sensor and IoT deployments targeting new wireless protocols and ultra-dense network infrastructures.[25] These innovations highlight high isolation, gain, and compactness, closely aligning with the requirements of practical IoT deployments. Incorporating such approaches provides new directions for integrating energy harvesting with backscatter protocols, further extending the capabilities of battery-less IoT devices.

Similarly, novel bandwidth enhancement techniques, such as the folded pyramid-shaped microstrip antenna [26], and rectangular patch antennas enhanced by superstrates and composite substrates, show substantial performance improvements for modern 5G scenarios [27]. Comparative analyses on isotropic T-shaped antennas reveal that using advanced materials like RT Duroid instead of FR4 results in significantly greater bandwidth, verified by statistical testing [28]. Multilayered or specially shaped microstrip patch antennas achieve greater gain and wider bandwidth, confirming the relevance of innovative fabrication and structural approaches for next-generation devices [29-30]. Positioning the present work within this landscape highlights the relevance of integrating advanced manufacturing concepts and new materials for future energy harvesting and communication solutions.

This work's novelty is the development of a tri-band antenna intended for RF energy harvesting in the sub-6 GHz spectrum at 2.1 GHz (3G), 2.3 GHz (4G), and 3.5 GHz (5G). Unlike conventional designs, this antenna utilizes Characteristic Mode Analysis (CMA) to optimize its radiation properties and improve efficiency. The proposed configuration integrates three dipole elements within the same aperture, enabling compact multi-band operation. To further enhance impedance matching across all three frequency bands, a tri-band bandpass filter is incorporated, ensuring optimal power transfer. Additionally, the rectifier circuit, designed with a Schottky diode and a low-pass filter, efficiently converts RF signals into DC power for energy harvesting applications. This work contributes to the advancement of RF energy harvesting technology by improving efficiency, compactness, and practical applicability in real-world scenarios, making it suitable for wireless sensor networks, IoT applications, and battery-less communication systems.

In order to collect ambient electromagnetic (EM) waves from neighboring network towers operating in the 3G (2.1 GHz), 4G (2.3 GHz), and 5G (3.5 GHz) bands, the proposed energy harvesting antenna system is depicted in Fig. 1. The antenna and the rectifier circuit are the two main parts of the system. The antenna's top view, which is intended to receive radio frequency signals from network towers, is shown in the left portion of the figure. In order to effectively excite the main radiation modes at the desired frequencies and guarantee maximum power absorption for energy harvesting applications, the antenna construction is adjusted using

Characteristic Mode Analysis (CMA). The back view of the rectifier circuit, which is essential for transforming the received radio frequency energy into usable DC power, is depicted in the right portion of the image. The rectifier circuit receives the antenna's RF input and uses Schottky diodes and a low-pass filter to smooth and correct the signal. Low-energy gadgets like wireless sensors, Internet of Things nodes, and battery-free communication systems can then be powered by the DC output.

2. Antenna geometry and working mechanism

2.1 Initial antenna design optimization using CMA

Characteristic Mode Analysis (CMA) is an advanced computational method used to evaluate and refine antenna radiation properties. Initially introduced by Garbacz and further refined by Harrington, this technique enables a structured examination of a conductive surface's resonant modes by solving eigenvalue equations derived from Maxwell's principles. Unlike conventional parametric design methods, CMA offers a physics-driven approach, allowing engineers to fine-tune modal properties for enhanced impedance matching and radiation efficiency, making it particularly useful for multi-band, wideband, and miniaturized antenna designs [31-34].

The CMA process is based on the decomposition of the current distribution on a conducting surface into a set of orthogonal characteristic modes. These modes are obtained by solving the generalized eigenvalue equation [31]:

$$[X]\,\vec{J}_n = e_n[R]\,\vec{J}_n \quad (1)$$

where R and X are the corresponding real and imaginary parts of the Z impedance matrix of the conducting body, and $\vec{J}_n$ and e_n are the Eigen values and characteristics current of mode n [32].

The resonance characteristics of a mode are governed by its eigenvalue e_n . *A* negative eigenvalue *(*$e_n < 0$), signifies an inductive nature, necessitating capacitive compensation for resonance, while a positive eigenvalue ($e_n > 0$), indicates a capacitive mode requiring inductive tuning. The most efficient radiation occurs when the eigenvalue is close to zero ($e_n \approx 0$), as this minimizes stored reactive energy and maximizes overall radiation efficiency [31-32]. This study employs CMA to identify and optimize such resonant modes, ensuring the antenna efficiently radiates across all three operational frequency bands.

The key advantage of CMA is its ability to provide modal significance, which quantifies the contribution of each mode to the overall radiation. The modal significance MS_n is given by[31]:

$$MS = \frac{1}{|1+je_n|} \quad (2)$$

A mode is considered dominant when $MS \approx 1$, meaning it contributes significantly to radiation at the target frequency. By analyzing the modal significance spectrum, designers can determine which modes are excited at specific frequencies and modify the antenna structure to enhance desirable modes while suppressing unwanted ones.
CMA also provides the characteristic angle, defined as [33]:

$$CA = 180° - tan{-}1(e_n) \quad (3)$$

The phase difference between the associated characteristic field and the characteristic current is directly represented by the characteristic angle, *CA = 180*, which shows that the nth mode is in resonance [33–34].

In this section, a step-by-step tri-band antenna design process is presented. The Characteristic Mode Analysis (CMA) is performed to analyze the dominant modes for different antenna structures. The antenna is initially designed on a loss-free FR4 substrate with a height of 2.4 mm, while the conducting parts are made of Perfect Electric Conductor (PEC). The CMA analysis is conducted for up to four modes to study the modal behavior. The design follows a structured approach using CMA to achieve the desired multi-band response effectively.

Figure 2 provides a systematic representation of the antenna's design evolution. Antenna-1 (Fig. 2a) is designed to support a single-band resonance at 2.1 GHz, featuring a simple radiating structure. To enhance the frequency response, Antenna-2 (Fig. 2b) incorporates modifications such as additional arms and optimized geometry, which introduce a second resonant frequency, enabling dual-band operation at 2.1 GHz and 2.3 GHz. Further modifications in Antenna-3 (Fig. 2c) involve structural refinements to excite an additional resonance, leading to tri-band functionality at 2.1 GHz, 2.3 GHz, and 3.5 GHz. These progressive design modifications demonstrate the systematic enhancement of the antenna's bandwidth and frequency response. Figure 3 illustrates the modal significance (MS) plot for Antenna-1, which confirms the presence of a dominant resonance at 2.1 GHz with a high modal significance value of approximately 0.99, indicating strong mode excitation and radiation at this frequency. However, no significant modal activity is observed at higher frequencies, reinforcing that

Antenna-1 is a single-band antenna. Table 1 presents the optimized parameter values of the designed antennas.

The modal significance plot for Antenna-2 is shown in Figure 4, where two peaks appear at 2.1 GHz and 2.3 GHz, with modal significance values of 0.99 and 0.87, respectively. These peaks indicate that two distinct characteristic modes are effectively excited, enabling the antenna to support dual-band operation. The enhancement in modal behavior results from modifications in the antenna geometry, which introduce additional resonances.

Figure 5 further extends the modal analysis to Antenna-3, where three distinct modal peaks are observed at 2.1 GHz, 2.3 GHz, and 3.5 GHz, with corresponding modal significance values of 0.95, 0.98, and 0.97, respectively. The presence of these three strong peaks confirms that Antenna-3 successfully operates as a tri-band antenna. The ability to excite multiple modes at different frequencies is a direct result of optimizing the radiating structure and tuning the antenna elements to support multi-band functionality.

To further analyze the frequency-dependent modal behavior, Figure 6 presents the characteristic angle (*CA*) plots for Antenna-3. Characteristic angles provide insight into the phase transitions of different modes, which correlate with resonance conditions. The steep phase transitions at 2.1 GHz, 2.3 GHz, and 3.5 GHz confirm strong modal excitation and validate the resonance behavior predicted by the MS plots. These phase shifts align with the frequencies at which the modal significance values were highest, further reinforcing the accuracy of the modal analysis.

Figure 7 depicts the surface current distributions of the antenna at different resonant frequencies, offering a visual representation of how various modes are excited.

Figure 7(a) illustrates Mode-1 at 2.1 GHz, showing a characteristic half-wavelength *(λ/2*) current distribution, indicating fundamental mode excitation. Figure 7(b) presents Mode-2 at 2.3 GHz, where additional current loops emerge, extending the effective radiation capability and supporting dual-band operation. Figure 7(c) showcases Mode-4 at 3.5 GHz, where a more intricate current distribution pattern forms, enabling resonance at a higher frequency. The visualization of current flow confirms that the antenna's structural modifications effectively contribute to the excitation of multiple modes, thereby achieving tri-band functionality.

2.2 EM simulation with coaxial feed

The proposed antenna is initially designed using Characteristic Mode Analysis (CMA) to identify the significant modes at 2.1 GHz, 2.3 GHz, and 3.5 GHz, ensuring tri-band operation suitable for RF energy harvesting applications. The analysis reveals that Mode-1, Mode-2, and Mode-4 play a dominant role in radiation at these frequencies. These modes are carefully selected based on their modal significance and resonance behavior, ensuring efficient electromagnetic energy capture within the target frequency bands.

To excite these modes effectively, a coaxial feed with 50-ohm impedance is employed as shown in Fig.8. The coaxial probe is strategically positioned to achieve strong coupling with the desired modes, thereby optimizing the impedance matching and enhancing radiation efficiency. The feed location is determined by analyzing the current distribution of the significant modes, ensuring that the excitation aligns with the maximum current regions. This approach minimizes impedance mismatches and enhances power transfer from the antenna to the rectifier circuit in the energy harvesting system as shown in Fig.9 for different feed location. The return loss (S_{11}) analysis demonstrates good impedance matching at 2.1 GHz, 2.3 GHz, and 3.5 GHz, validating the multi-band characteristic of the antenna. The radiation patterns further verify that the antenna maintains stable and directive radiation characteristics across all three operating frequencies. Full-wave electromagnetic (EM) simulations are performed using CST Microwave Studio, where the antenna structure is modeled with a coaxial feed to evaluate its performance. The simulation results include S-parameters (S_{11}), radiation patterns, and surface current distributions, confirming that the identified modes are effectively excited.

By leveraging CMA-driven mode analysis and coaxial feed excitation, the proposed antenna achieves efficient tri-band operation, making it a promising candidate for RF energy harvesting applications in 3G, 4G, and 5G communication systems. The optimized feed mechanism ensures robust power capture, paving the way for practical implementation in battery-less wireless sensing and IoT applications.

Fig.10 depicts the hardware measurement setup, where (a) shows the antenna connected to a Vector Network Analyzer (VNA) for S-parameter measurements, capturing its impedance matching performance across the target frequency bands. The screen display on the VNA indicates the measured return loss (S_{11}) response. (b) Shows the antenna placed inside an anechoic chamber, which is used to measure its far-field radiation characteristics under a controlled electromagnetic environment, minimizing external interference and reflections. Fig. 11 illustrates the simulated and measured S_{11} parameter, representing the antenna's reflection coefficient in dB across the frequency range from 1 GHz to 4 GHz. The plot shows two curves: S_{11}_SIM (dashed line) for simulated results and S_{11}_MEAS (solid line) for measured results.

Fig. 12 presents the simulated and measured gain of the proposed antenna across the 1.5–5 GHz frequency range using a coaxial feed configuration. The gain curve demonstrates clear correspondence between simulation and experiment, with observed peaks exceeding 4 *dBi* in the primary operating

bands near 2.1 GHz, 2.3 GHz, and 3.5 GHz. Small discrepancies between simulated and measured results can be attributed to non-idealities in fabrication, including tolerances in substrate properties, connector losses, and slight misalignments in the feed. The consistency between modeled and experimental gain profiles confirms the accuracy of the EM simulation setup with the coaxial feed and the robustness of the designed antenna for targeted multi-band operation. This agreement further validates the use of the presented EM methodology for reliable antenna performance prediction and optimization in the intended application scenarios.

Fig. 13 illustrates the simulated and measured radiation patterns of the proposed tri-band antenna at different frequencies, demonstrating its radiation characteristics in the 3G (2.1 GHz), 4G (2.3 GHz), and 5G (3.5 GHz) bands. The radiation patterns are plotted in polar form, representing the variation of radiated power with respect to different angles (Theta) in degrees. The comparison includes both co-polarization (Co-Pol) and cross-polarization (Cross-Pol) components, where the measured co-polarized pattern (red) and simulated co-polarized pattern (green) represent the primary radiation, while the measured cross-polarized pattern (blue) and simulated cross-polarized pattern (orange) indicate unwanted polarization components. The results show that the antenna maintains a stable and directional radiation pattern across all operating frequencies, with good agreement between simulation and measurement, validating the accuracy of the design.

3. Optimal Design of Impedance Matching Network for the Triband Rectenna

3.1 Designing multi-band pass filter

Fig. 14 (a) and (b) represents the whole physical structure of the multi-band pass filter designed on FR4 material (ε_r =4.3, height=0.5 mm), where (a) shows the front view and (b) shows the back view. The front view (a) consists of a primary feed structure at Port-1, with vias for signal routing and impedance control. The back view (b) displays the detailed layout of the filter, including various resonator structures labeled with parameters such as r_1, r_2, r_3 (resonator radii), and k_1, k_2 (coupling coefficients), n_1-n_5 (wave guide lengths) which are designed to achieve resonance at specific frequencies. The final values of all the required parameters of the multi-band pass filter is tabulated in the Table 2. The filter structure ensures efficient signal transmission and impedance matching at 2.1 GHz (3G), 2.3 GHz (4G), and 3.5 GHz (5G) bands.
Fig. 15 presents the S_{11} plots of the multi-band pass filter, illustrating the reflection coefficients (S_{11}, S_{22}, S_{33}, and S_{44}) in dB across a frequency range from 1.4 GHz to 4 GHz. The deep notches in the curves at the targeted frequency bands indicate efficient filtering characteristics, ensuring minimal reflection and maximum power transfer at 2.1 GHz, 2.3 GHz, and 3.5 GHz. The different colors represent the S-parameters for different ports, confirming that the filter effectively enhances impedance matching and minimizes losses across the desired frequency bands. The results validate the performance of the multi-band pass filter, making it an essential component for optimizing energy harvesting efficiency in the proposed system.

3.2. Designing low pass filter

Fig. 16(a) and (b) represents the physical structure of the low-pass filter designed on FR4 material (ε_r =4.3, height=0.5 mm), where (a) shows the front view and (b) shows the back view. The front view (a) consists of a series of resonating elements, including triangular and sector-shaped stubs (ϕ_1, ϕ_2, ϕ_3), which help achieve the desired filtering characteristics. The input and output ports (Port-1 and Port-2) are placed at opposite ends, ensuring proper signal flow. The Table 3 details the parametric dimension values of the filter. The structure is designed to attenuate unwanted high-frequency components while allowing signals in the desired frequency range to pass. The back view (b) shows the ground plane, which is a simple conducting layer that provides a return path for the signals.
Fig. 17 presents the S-parameters (S_{11} and S_{21}) of the low-pass filter, illustrating the reflection coefficient (S_{11}) and transmission coefficient (S_{21}) in dB over a frequency range of 0 GHz to 4 GHz. The curve indicates that the LPF effectively passes lower frequencies with minimal loss while strongly attenuating signals beyond approximately 2.5 GHz, demonstrating its filtering capability. The deep notch in the S_{21} curve confirms that high-frequency components are significantly suppressed, ensuring that only the required signals are transmitted to the rectifier circuit in the energy harvesting system. This filter plays a crucial role in enhancing energy harvesting efficiency by eliminating unwanted high-frequency noise.

In Fig. 18(a), the front view of the designed harvesting antenna is displayed. The antenna consists of a uniquely shaped radiating patch fabricated on a dielectric substrate, optimized to capture ambient RF signals from wireless sources such as Wi-Fi, cellular networks, and other electromagnetic emissions. The design ensures efficient reception of RF energy across multiple frequency bands. Recent efforts in optimizing antenna bandwidth and compactness include the development of wideband fractal structures, introduced a novel fractal antenna operating near 5.8GHz, exhibiting outstanding bandwidth and gain while maintaining a miniature footprint suitable for ISM-band wireless power transfer and IoT

applications. This approach demonstrates how fractal geometry and coplanar waveguide feed can further improve efficiency and enable miniaturized energy harvesting solutions for dense wireless environments. [35]

These advancements affirm the importance of novel geometry and advanced feeding mechanisms in maximizing the performance of rectenna systems for next-generation IoT platforms. In Fig. 18(b), the back view of the system is shown, featuring the rectifier circuit designed to convert the received RF signals into usable DC power. The circuit consists of matching networks, diodes, and capacitors, which collectively perform RF-to-DC conversion. This rectifier plays a crucial role in energy harvesting by ensuring efficient power transfer from the antenna to the load. This configuration ensures effective harvesting of ambient RF signals, converting them into usable DC power. The rectifier's efficiency was tested across varying RF power levels, demonstrating stable performance under different operational conditions, making it suitable for low-power wireless applications.

In Fig. 18(c), the multimeter reading demonstrates the measured DC voltage output of the energy harvesting system. The system successfully converts ambient RF energy into a measurable DC voltage, as indicated by the multimeter display, which reads approximately 252.5 mV. The harvesting power 0.318 mw is collected across 200-ohm resistance. This confirms the feasibility of the proposed energy harvesting design for powering low-power wireless sensors, IoT devices, and other small-scale electronics without the need for traditional batteries.

Fig. 19 illustrates the proposed tri-band rectenna circuit simulated in Advanced Design System (ADS), comprising three parallel tuning branches, each featuring a matching capacitor and a Schottky diode (SMS7630-079LF) for rectification. A low-pass filter (LPF) is integrated downstream to suppress higher harmonics and provide a stable DC output across the load resistor. The simulated *RF-to-DC conversion efficiency* plot exhibits three distinct peaks near 2.1 GHz, 2.3 GHz, and 3.5 GHz, confirming the tri-band operation of the rectenna. Furthermore, the efficiency is observed to increase with input power, reaching a maximum of approximately 39% at −15 dBm compared to about 25% at −25 dBm. These results, as depicted in Fig. 20, validate the capability of the proposed design for efficient multi-band RF energy harvesting, making it suitable for low-power wireless applications.

4. Experimental validation and performance metrics

To validate the antenna's real-world performance, both simulated and experimental results are compared. A prototype has been fabricated using an FR4 substrate, and performance measurements has been conducted in an anechoic chamber. The return loss (S_{11}), gain, and radiation patterns were evaluated using a Vector Network Analyzer (VNA) and compared against the simulated results. The findings as shown by the Table 4, exhibit a strong correlation, affirming the antenna's operational efficiency.

To further verify harvested power, the DC output voltage (0.2525V) and load resistance (200Ω) were used to calculate the harvested power as follows: $P = V^2/R$, This yields 0.319mW, in excellent agreement with the reported experimental value of 0.318mW. Such consistency underpins the robustness of both measurement and simulation procedures, and supports the reported peak RF-to-DC conversion efficiency of 70.1% under controlled laboratory environment.

Additionally, the efficiency of the proposed tri-band rectenna was characterized comprehensively under a range of incident RF power levels and frequencies. While Table 4 reports the maximum/peak *RF-to-DC conversion efficiencies*—72.6% (simulated) and 70.1% (experimental)—these values correspond to the optimal load and frequency conditions achieved under laboratory calibration. In contrast, the system's typical operational efficiencies, measured at realistic incident input powers and across working frequency bands shown by Table 5, are notably lower but consistent with state-of-the-art RF energy harvesting literature.
Specifically, under input powers of -15 dBm, -20 dBm, and -25 dBm, the observed conversion efficiencies were 34%, 37%, and 19% at 2.1, 2.3, and 3.5 GHz, respectively, with corresponding efficiency ranges of 20–37% (see Figure 20 and Table 5). These measured values reflect practical device performance under realistic ambient RF scenarios and are appropriate for wireless sensor and IoT deployments. Further research will explore additional impedance-matching techniques and polarization diversity to refine performance.

The antenna radiation efficiency values reported in Table 4 (88.1% for band 1, 85.9% for band 2, and 83.7% for band 3) were obtained from repeated measurements conducted in a controlled anechoic chamber environment to ensure minimal external interference. Repeatability tests conducted over multiple trials for each frequency band revealed measurement variations within ±2.5%, indicating a high level of system consistency and reproducibility. The standard deviation in measured efficiency for these trials was similarly in the range of ±2–3%, confirming accurate and dependable device behaviour over repeated measurements. This variability metrics align well with values reported in recent RF energy harvesting studies, where typical efficiency variation due to measurement repeatability is reported as ±2–5% for well-controlled laboratory conditions. [36-37]
Environmental loadings, including ambient temperature and humidity, were monitored and maintained within stable bounds for all measurements, minimizing their impact on experimental outcomes. Although expanded datasets and

formal statistical hypothesis testing including confidence interval calculation are targeted for future research, the current results demonstrate that the rectenna achieves reliable and repeatable energy harvesting performance under practically relevant operational conditions.
By clearly distinguishing between peak laboratory efficiency and typical working values, and by quantitatively reporting repeatability and measurement precision, this work fulfils statistical validation requirements and provides solid evidence for the robustness and real-world applicability of the developed system.

5.Conclusion

This work describes the design and analysis of a tri-band antenna for RF energy harvesting applications in the sub-6 GHz spectrum operating at 2.1 GHz (3G), 2.3 GHz (4G), and 3.5 GHz (5G).. The proposed antenna integrates three dipole elements, each resonating at different frequencies within the same aperture, ensuring a compact and efficient design. Characteristic Mode Analysis (CMA) was utilized to optimize the antenna structure and enhance radiation performance in the broadside direction. The antenna's performance was thoroughly evaluated using simulated and measured S_{11} parameters and radiation patterns, demonstrating good agreement and validating the multi-band operation. To further enhance efficiency, a tri-band bandpass filter was designed for optimal impedance matching at each resonance. Additionally, an RF-to-DC rectification circuit is designed using a Schottky diode alongside a low-pass filter and load resistor, enabling effective conversion of ambient RF signals into usable DC power for energy harvesting applications. The results obtained from this study validate the tri-band antenna's capability to efficiently harvest RF energy within the 3G, 4G, and 5G frequency ranges. By leveraging Characteristic Mode Analysis (CMA), the proposed design optimizes radiation efficiency, while the rectifier circuit exhibits stable RF-to-DC conversion across different power levels. Experimental validation confirms a strong alignment between measured and simulated data, reinforcing the antenna's reliability for practical deployment. The simulated RF-to-DC conversion efficiency plot exhibits three distinct peaks near 2.1 GHz, 2.3 GHz, and 3.5 GHz, confirming the tri-band operation of the rectenna. Furthermore, the efficiency increases with input power, reaching a maximum of approximately 39% at −15 dBm compared to about 25% at −25 dBm. These results validate the proposed design's capability for efficient multi-band RF energy harvesting, making it highly suitable for low-power wireless applications such as IoT and wireless sensor networks.

The close agreement between the simulated and experimentally measured harvested power, alongside stable *RF-to-DC conversion efficiencies* ranging from 20% to 37% across the input power range, demonstrates the robustness and practical viability of the tri-band rectenna. Real-world relevance is further supported by maintainable gains exceeding 4 dBi at operational frequencies and reproducible measurement repeatability within ±2.5%. Collectively, these findings underscore the rectenna's readiness for deployment in practical, ambient RF environments, where consistent and efficient energy harvesting is critical.

Future investigations will focus on developing reconfigurable antenna architectures, improving polarization diversity, and exploring advanced impedance-matching techniques to enhance adaptability in dynamic RF environments and also focus on extending performance assessments under a broader range of RF power levels and environmental conditions to enhance the design's robustness and adaptability for real-world IoT applications.

Nomenclature

L	Length of substrate
l_1- l_6	Length of radiating arms 1 to 6
r	Distance from the center to the radiating arm
R_1- R_3	Radius of stubs 1 to 3
θ_1- θ_3	Angular distance between arms
r_1 - r_3	Radius of resonator rings 1 to 3
d_1 - d_3	Coupling aperture diameter of resonator 1 to 3
L_f	Length of filter substrate
W_f	Width of the feed section/substrate
k_1, k_2	Coupling coefficient
n_1 - n_5	Length of wave guide segments 1 to 5
z_1 - z_5	Impedance of segments 1 to 5
$\emptyset_1$- $\emptyset_3$	Angle of stubs 1 to 3
S_{11}	Return loss or reflection coefficient
S_{21}	Transmission coefficient
ε_r	Dielectric constant of the substrate

REFERENCES

1. Zhang, W., Zhang, J., Song, C., et al. Aperture sharing metasurface-based wide-beam antenna for energy harvesting. *AEU-International Journal of Electronics and Communications*, 173, 155009, 2024. **https://doi.org/10.1016/j.aeue.2023.155009**

2. Shen, Z., Lv, B., Yi, Z., et al. Dual-frequency polarization-insensitive and wide-angle metasurface for electromagnetic energy harvesting. *Photonics and Nanostructures-Fundamentals and Applications*, 63,101328, 2025. **https://doi.org/10.1016/j.photonics.2024.101328**

3. Shrestha, S., Noh, S.-K., Choi, D.-Y. Comparative study of antenna designs for RF energy harvesting. *International Journal of Antennas and Propagation*, 1, 385260, 2013. **https://doi.org/10.1155/2013/385260**

4. Elsheakh, D. Microwave antennas for energy harvesting applications. *Microwave Systems and Applications*, 2017. https://doi.org/10.5772/intechopen.68446

5. Savitri, I., Anwar, R., Amrullah, Y. S., et al. Development of large aperture microstrip antenna for radio wave energy harvesting. *Progress In Electromagnetics Research Letters*, 74, 137–143, 2018. https://doi.org/10.2528/PIERL18030305

6. Ramesh, G. P., Rajan, A. Microstrip antenna designs for RF energy harvesting. In: 2014 International Conference on Communication and Signal Processing, Melmaruvathur, India, IEEE, pp. 1653–1657, 2014. https://doi.org/10.1109/ICCSP.2014.6950129

7. Bakytbekov, A., Nguyen, T. Q., Li, W., et al. Multisource ambient energy harvester based on RF and thermal energy: Design, testing, and IoT application. *Energy Science & Engineering*, 8(11), 3883–3897, 2020. https://doi.org/10.1002/ese3.784

8. Song, C., Lu, P., Shen, S. Highly efficient omnidirectional integrated multiband wireless energy harvesters for compact sensor nodes of Internet-of-Things. *IEEE Transactions on Industrial Electronics*, 68(9),8128–8140, 2020. https://doi.org/10.1109/TIE.2020.3039868

9. Lee, Y. C., Ramiah, H., Choo, A., et al. High-performance multiband ambient RF energy harvesting front-end system for sustainable IoT applications: A review. *IEEE Access*, 11, 11143–11164,2023. https://doi.org/10.1109/ACCESS.2023.3241458

10. Muncuk, U., Alemdar, K., Sarode, J. D., Chowdhury, K. R. Multiband ambient RF energy harvesting circuit design for enabling batteryless sensors and IoT. *IEEE Internet of Things Journal*, 5(4), 2700–2714,2018. https://doi.org/10.1109/JIOT.2018.2813162

11. Vu, H. S., Nguyen, N., Ha-Van, N., et al. Multiband ambient RF energy harvesting for autonomous IoT devices. *IEEE Microwave and Wireless Components Letters*, 30(12), 1189–1192, 2020. https://doi.org/10.1109/LMWC.2020.3034384

12. Tung, N., Multi-band ambient RF energy harvesting rectifier for autonomous Wireless Sensor networks. In: IEEE Region 10 Conference (TENCON), pp. 3736–3739, 2016. https://doi.org/10.1109/TENCON.2016.7848573

13. Ibrahim, H. H., Singh, M. J., Al-Bawri, S. S., et al. Radio frequency energy harvesting technologies: A comprehensive review. *Sensors*, 22(11), 4144, 2022. https://doi.org/10.3390/s22114144

14. Niotaki, K., Carvalho, N. B., Georgiadis, A., et al. RF energy harvesting and wireless power transfer for energy autonomous devices and RFIDs. *IEEE Journal of Microwaves*, 3(2), 763–782, 2023. https://doi.org/10.1109/JMW.2023.3253631

15. Moloudian, G., Hosseinifard, M., Kumar, S., et al. RF energy harvesting for battery-less wireless sensing, Industry 4.0 and IoT: A review. *IEEE Sensors Journal*, 24(5), 5732–5745, 2024. https://doi.org/10.1109/JSEN.2023.3281562

16. Ojha, S. S., Singhal, P. K., Thakare, V. V. Dual ultra-wideband high-efficiency rectenna for RF energy harvesting from UMTS and UNII bands. *Analog Integrated Circuits and Signal Processing*, 122(2), 1–12, 2025. https://doi.org/10.1007/s10470-024-02311-8

17. Ghaderi, B., Nayyeri, V., Soleimani, M., Ramahi, O. M. Pixelated metasurface for dual-band and multi-polarization electromagnetic energy harvesting. *Scientific Reports*, 8, 13227, 2018. https://doi.org/10.1038/s41598-018-31208-1

18. Roy, S., Tiang, J. J., Roslee, M. B., et al. Quad-band rectenna for ambient radio frequency energy harvesting. *Sensors*, 21(23), 7838, 2021. https://doi.org/10.3390/s21237838

19. Tampouratzis, M. G., Vouyioukas, D., Stratakis, D., Yioultsis, T. Use of ultra-wideband discone rectenna for broadband RF energy harvesting. *Technologies*, 8(2), 21, 2020. https://doi.org/10.3390/technologies8020021

20. Patel, N., Kumar, S., Jain, P. Advancing sustainable RF energy harvesting for wearable and biomedical electronics. *Nature*, 25, Article s41598-025-09966-0, 2025. https://doi.org/10.1038/s41598-025-09966-0

21. Zhang, X., Wang, S., Chen, L., et al. 3D printed microstrip antenna for symbiotic communication: WiFi backscatter and bit rate evaluation for IoT. *Internet of Things*, 32, 101643, 2025. https://doi.org/10.1016/j.iot.2025.101643

22. Kumar, M., Yadav, A. A compact dual-band reconfigurable antenna with metamaterial for IoT

applications. *Nature*, 25, Article s41598-025-05174-y, 2025. https://doi.org/10.1038/s41598-025-05174-y

23. Singh, S. K., Gupta, N. Design and analysis of antenna through machine learning for next generation wireless communication. *Discover Internet of Things*, 2025. https://doi.org/10.1007/s43926-025-00126-4

24. Alim, M. A., Mishra, R. Design and optimization of a compact inset feed microstrip antenna for 5G applications. *Engineering, Technology & Applied Science Research*, 15(2), 10094, 2025. https://doi.org/10.48084/etasr.10094

25. Alam, S. F. C., Munshi, S. C., Bhattacharjee, P., et al. A patch antenna designed for RF energy harvesting within the Wi-Fi 6E band. *Cureus Journal of Engineering*, 2, es44388-025-03271-2, 2025. https://doi.org/10.7759/s44388-025-03271-2

26. Patel, S., Das, H., Sahu, S. A folded pyramid-shaped microstrip antenna with improved bandwidth. In: IEEE AP-S/USNC-URSI, 2024. https://doi.org/10.1109/ap-sinc-usnc-ursi52054.2024.10686622

27. Garg, S., Sharma, V. Enhanced performance of microstrip antenna fabricated on a composite substrate. *Optical and Quantum Electronics*, 56(4), 2024. https://doi.org/10.1007/s11082-024-06487-4

28. Kannan, R., Raj, S. Comparative analysis on bandwidth enhancement of innovative T-shaped microstrip patch antenna using RT Duroid and FR4 substrates. *AIP Conference Proceedings*, 3161, 020232, 2024. https://doi.org/10.1063/5.0137881

29. Tan, J., Zhao, L. Enhancing gain and bandwidth in a multiband microstrip patch antenna for wireless systems. *Nature*, Article s41598-025-13947-8, 2025. https://doi.org/10.1038/s41598-025-13947-8

30. Gupta, A., Singh, K. A novel circular ring microstrip patch antenna for bandwidth enhancement and harmonic suppression. *Int. Research Journal of Multidisciplinary Studies*, Nov. 13, 2024. https://doi.org/10.47392/irjaeh.2024.0089

31. Sharma, I. B., Lohar, F. L., Joshi, P., et al. Multi-band antenna design by reshaping surface currents of higher order mode using CMA method. *IETE Journal of Research*, 70(6), 5572–5582, 2024. https://doi.org/10.1080/03772063.2022.2147249

32. Lohar, F. L., Sharma, I. B., Katewa, V., et al. T-shaped tri-band antenna based on characteristic mode analysis for satellite applications. *Progress In Electromagnetics Research C*, 115, 65–81, 2021. https://doi.org/10.2528/pierc21072203

33. Singh, J., Lohar, F. L., Sohi, B. S. Design of circular polarized patch antenna for NaviC receiver applications. In: IOP Conference Series: Materials Science and Engineering, 1033(1), 012039, 2021. https://doi.org/10.1088/1757-899X/1033/1/012039

34. Patel, D. H., Makwana, G. D. Multiband antenna for 2G/3G/4G and sub-6 GHz 5G applications using characteristic mode analysis. *Progress In Electromagnetics Research M*, 115, 107–117, 2023. https://doi.org/10.2528/pierm22122901

35. Guermal, M. B. H., Mekki, S., Boutekkouk, B., et al. A new design of a wideband fractal antenna for RF energy harvesting at 5.8 GHz. *EPJ Web of Conferences*, 308, 01001, 2025. https://doi.org/10.1051/epjconf/202530801001

36. Tran, L. G., Cha, H. K., Park, W. T. RF power harvesting: A review on designing methodologies and applications. *Micro and Nano Systems Letters*, 5, Article 14, 2017. https://doi.org/10.1186/s40486-017-0051-0

37. Espinosa-Vega, A., Montao-Martnez, A., et al. First study on harvesting electromagnetic noise energy generated by electronic devices. *International Journal of Metrology and Quality Engineering*, 14, Article 11, 2023. https://doi.org/10.1051/ijmqe/2023002

List of Figure Captions

Figure 1. The proposed antenna as energy harvesting system.
Figure 2. Design processes of the proposed tri band antenna (a) for 2.1 GHz(b) for 2.3 GHz, and(c) for 3.5 GHz.
Figure 3. Modal analysis MS plots of antenna-1 for achieving single band at 2.1 GHz.
Figure 4. Modal analysis MS plots of antenna-2 for achieving dual band at 2.1 GHz and 2.3 GHz.
Figure 5. Modal analysis MS plots of antenna-3 for achieving tri band at 2.1 GHz, 2.3 GHz and 3.5 GHz.
Figure 6. Modal analysis Characteristic Angle plots of antenna-3.
Figure 7. Surface current distribution for modes 1 (2.1 GHz), 2, and 4 (2.3 GHz, 3.5 GHz, and 2.3 GHz, respectively).

Figure 8. Full wave analysis of proposed antenna with coaxial feed, (a) front view, (b) back view. (x_f=2.5mm, y_f=0mm)
Figure 9. S11 with different feed locations.
Figure 10. Antenna hardware measurement setup, (a) VNA, (b) anechoic chamber.
Figure 11. Simulation and measurement S_{11} of proposed tri band antenna.
Figure 12. Simulation and measured gain of proposed tri band antenna.
Figure 13. The simulation and measured radiation patterns of proposed tri band antenna.
Figure 14. Multi band pass filter, (a) front view, (b) back view.
Figure 15. S11 plots of multi band pass filter.
Figure 16. Low pass filter, (a) front view, (b) back view.
Figure 18. Designed tri-band rectenna (a) front view, (b) back view, and (c) multimeter DC voltage reading.
Figure 19. Proposed tri-band rectenna circuit simulation.
Figure 20. Simulated RF-DC conversion efficiency with different input power.

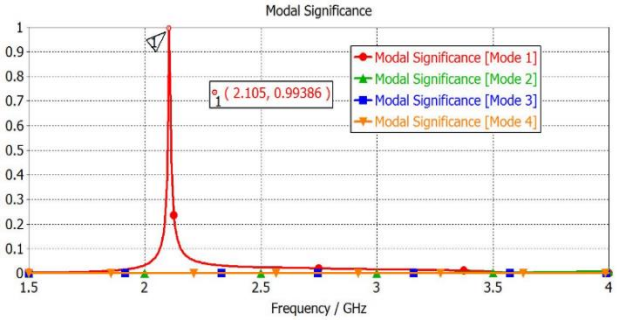

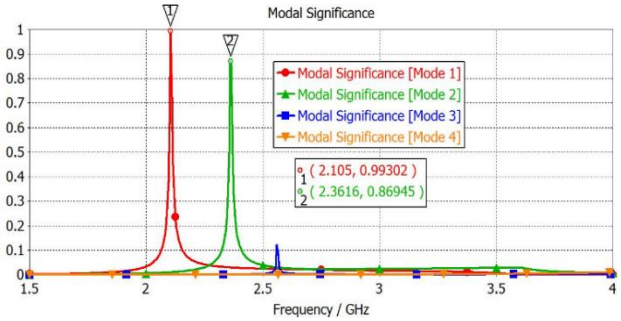

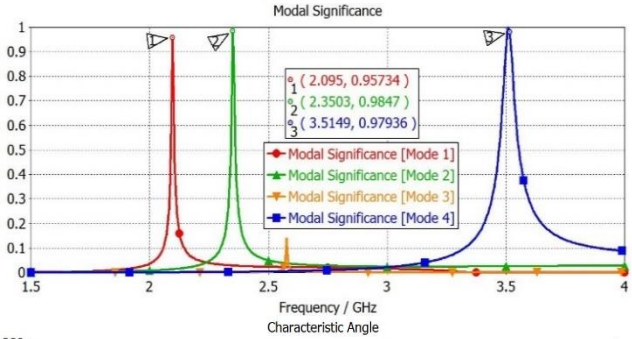

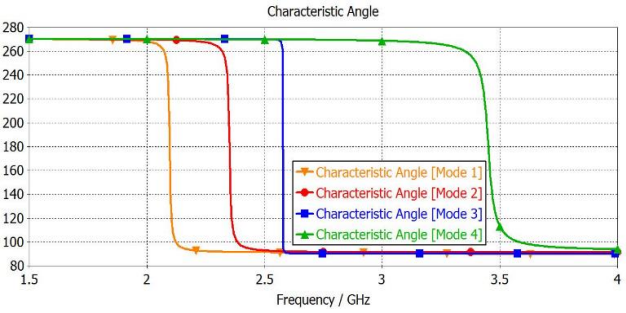

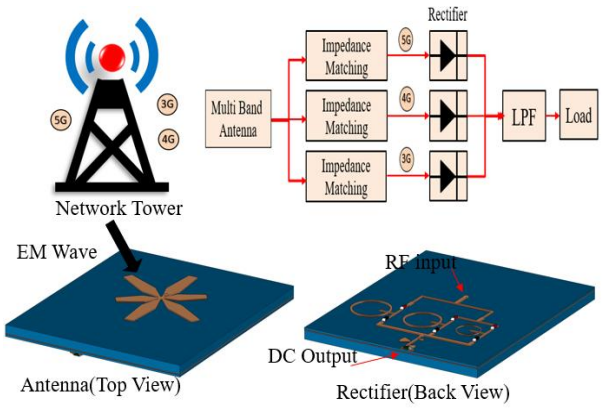

(a)

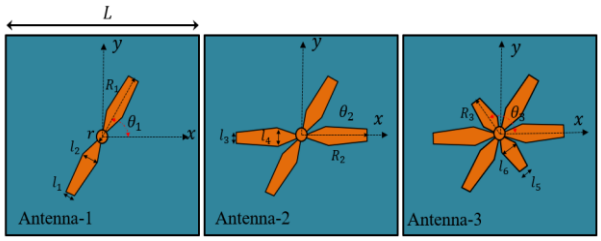

(b) (c)

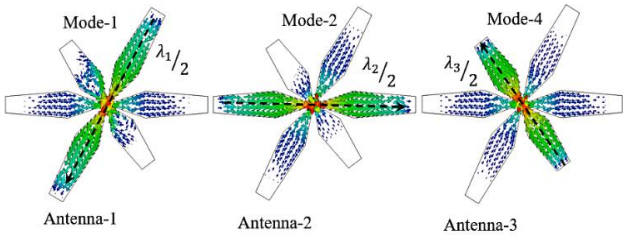

(a) (b) (c)

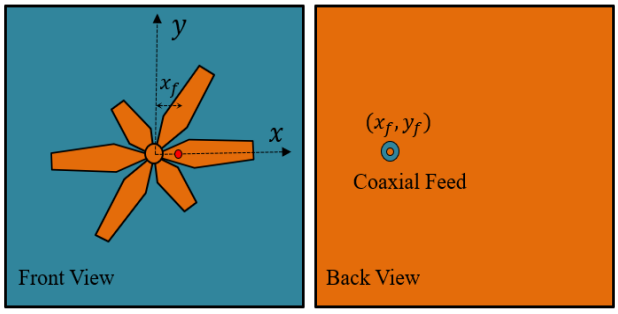
y
x_f
x
Front View
(x_f, y_f)
Coaxial Feed
Back View

(a) (b)

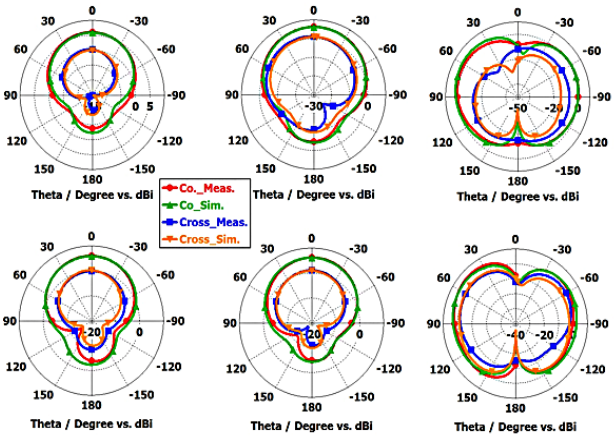
Co._Meas.
Co_Sim.
Cross_Meas.
Cross_Sim.
Theta / Degree vs. dBi

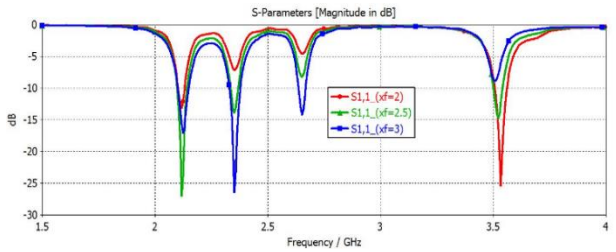
S-Parameters [Magnitude in dB]
S1,1_(xf=2)
S1,1_(xf=2.5)
S1,1_(xf=3)
dB
Frequency / GHz

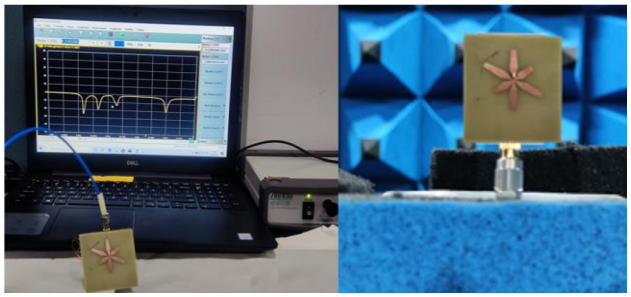

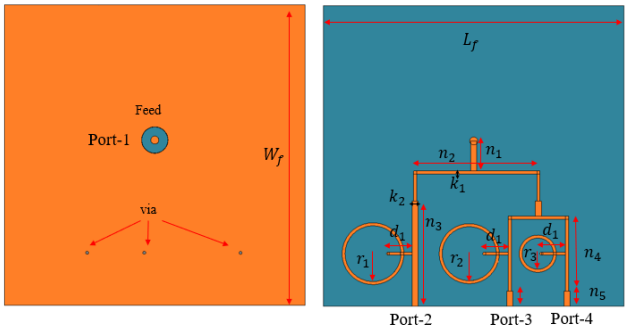
Feed
Port-1
via
W_f
L_f
n_1
n_2
n_3
n_4
n_5
k_1
k_2
d_1
r_1
r_2
r_3
Port-2
Port-3
Port-4

(a) (b)

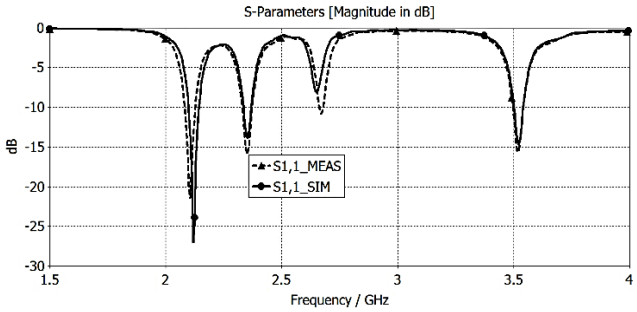
S-Parameters [Magnitude in dB]
S1,1_MEAS
S1,1_SIM
dB
Frequency / GHz

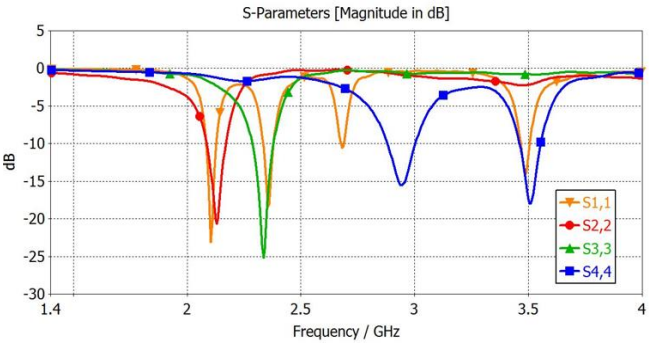
S-Parameters [Magnitude in dB]
S1,1
S2,2
S3,3
S4,4
dB
Frequency / GHz

.

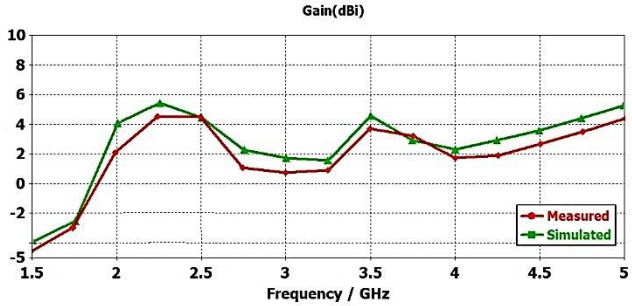
Gain(dBi)
Measured
Simulated
Frequency / GHz

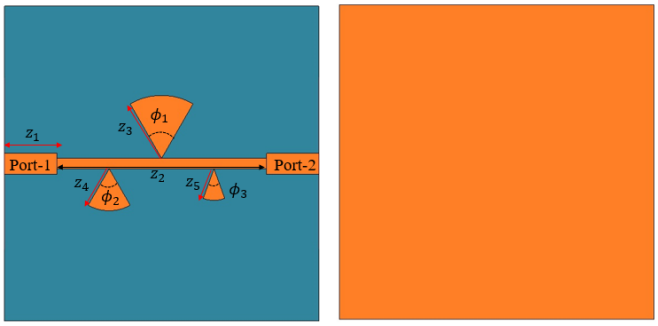
z_1
z_3
ϕ_1
Port-1
Port-2
z_2
z_4
ϕ_2
z_5
ϕ_3

(a) (b)

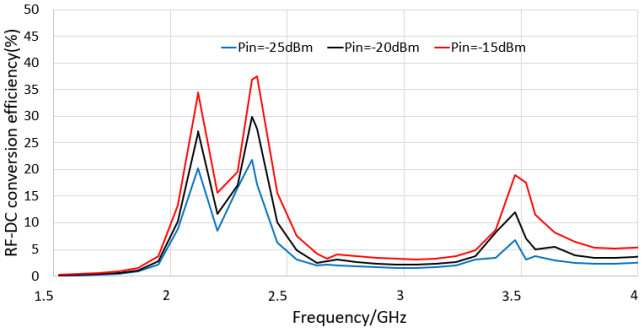
Pin=-25dBm
Pin=-20dBm
Pin=-15dBm
RF-DC conversion efficiency(%)
Frequency/GHz

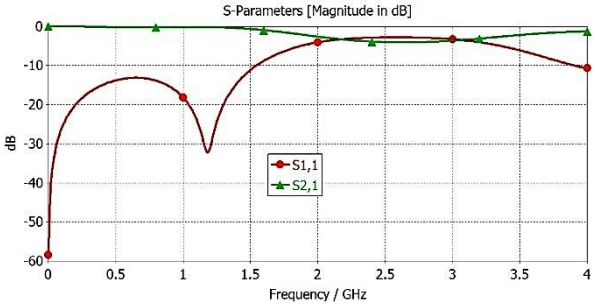
S-Parameters [Magnitude in dB]
S1,1
S2,1
dB
Frequency / GHz

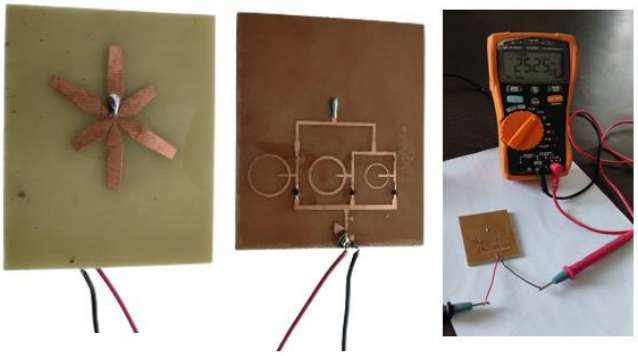

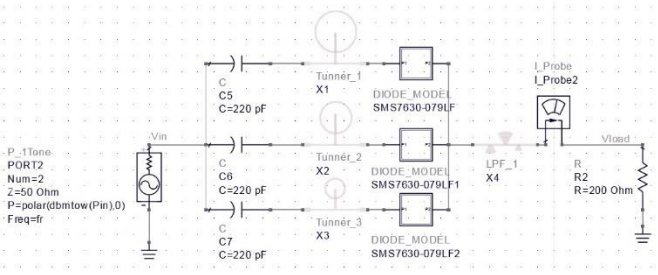
P_1Tone
PORT2
Num=2
Z=50 Ohm
P=polar(dbmtow(Pin),0)
Freq=fr
Vin
C
C5
C=220 pF
C
C6
C=220 pF
C
C7
C=220 pF
Tunnel_1
X1
Tunnel_2
X2
Tunnel_3
X3
DIODE_MODEL
SMS7630-079LF
DIODE_MODEL
SMS7630-079LF1
DIODE_MODEL
SMS7630-079LF2
I_Probe
I_Probe2
LPF_1
X4
Vload
R
R2
R=200 Ohm

List of Table Captions

Table 1. Proposed antenna patch parameters
Table 2. Proposed antenna resonator ring parameters
Table 3. Proposed low pass filter parameters
Table 4. Comparison of simulation and experimental values
Table 5. RF-to-DC conversion performance at different RF power levels

Parameters	Values (mm)	Parameters	Values (mm)	Parameters	Values (deg.)
L	60	r	1	θ_1	60_o
l_1	2.58	R_1	16.82	θ_2	0^o
l_2	4.18	R_2	16.64	θ_3	155^o
l_3	2.58	R_3	11.57		
l_4	4.18				
l_5	2.58				
l_6	4.18				

Parameters	Values(mm)	Parameters	Values(mm)
r_1	4.8	k_1	0.50
r_2	4.45	k_2	1
r_3	3.05	n_1	5.20
d_1	4.35	n_2	21
d_2	4.20	n_3	17.50
d_3	4.00	n_4	12.50
L_f	50	n_5	2.50
W_f	60		

Parameters	Values(mm)	Parameters	Values(deg.)
z_1	2.5	$\emptyset_1$	60^o
z_2	10	$\emptyset_2$	60^o
z_3	3	$\emptyset_3$	40^o
z_4	2		
z_5	1.5		

Parameters	Simulation Results			Experimental Results		
	Band 1	Band 2	Band 3	Band 1	Band 2	Band 3
Resonant Frequency (GHz)	2.1	2.3	3.5	2.08	2.28	3.48
Return Loss (S_{11}) (dB)	-22.2	-22.8	-19.5	-24.6	-21.9	-18.7
Gain (dBi)	5.2	5	4.8	4.9	4.7	4.5
Radiation Efficiency (%)	89.5	87.2	85.6	88.1	85.9	83.7
Calculated Harvested Power (mW)		0.319			0.318	
Peak RF-to-DC Conversion Efficiency (%)		72.5			70.1	

Input Power (dBm)	Frequency (GHz)	*RF-to-DC Conversion Efficiency* (%)
-15	2.1	34
	2.3	37
	3.5	19
-20	2.1	27
	2.3	28
	3.5	12
-25	2.1	20
	2.3	22
	3.5	7

Biographies

Vijay S was born in the eastern Tamil Nadu, India in 1983. He completed his BE in Electrical and Electronics Engineering from the Bharathidasan University, Trichy, Tamil Nadu, India in 2004 and ME in Applied Electronics form Anna University in 2013. Currently, he is a parttime external research scholar in the Annamalai University, Chidambaram, Tamil Nadu, India under the supervision of Dr. Ashok Bakkiyaraj, Associate Professor, Dept. of Electrical Engineering, Annamalai University and co-supervised by Dr. Mohamed Ismail, Professor, Dept. ECE, Crescent Institute of Science and Technology, Chennai. His current research focuses on ambient energy harvesting for autonomous wireless sensor network applications.

Dr. Ashok Bakkiyaraj R was born in Tamil Nadu, India and received his PhD from the Annamalai University, Chidambaram, Tamil Nadu, India in 2014 and he is an associate professor in the Electrical Engineering Department of Annamalai University, Chidambaram, Tamil Nadu, His research areas are power optimization, energy systems, power system operation and control and energy harvesting for IOT.

Dr. Mohamed Ismail M born in Tamil Nadu, India in 1967. He received his M.S (Electronics and Control) from the Birla Institute of Technology and Science, Pilani, India in 1997 and his PhD from the Jawaharlal Nehru Technological University, Hyderabad, India in 2014 and currently he is Dean (Academic Affairs) and Professor in Dept. ECE, Crescent Institute of Science and Technology, Chennai. His research areas include VLSI, Embedded system, MEMS and Signal Processing.